Supporting Information

Improved tumor targeting and penetrating by dual-functional poly(amidoamine) dendrimer for the therapy of triple-negative breast cancer

Changliang Liu,[ab] Houqian Gao,[ab] Zijian Zhao,[a] Iman Rostami,[a] Chen Wang,*[ab] Ling Zhu,*[ab] and Yanlian Yang*[ab]

[a] CAS Key Laboratory of Standardization and Measurement for Nanotechnology, CAS Key Laboratory of Biological Effects of Nanomaterials and Nanosafety, CAS Center for Excellence in Nanoscience, National Center for Nanoscience and Technology, Beijing 100190, P. R. China.

[b] University of Chinese Academy of Sciences, Beijing, 100049, P.R. China.

* Corresponding authors: wangch@nanoctr.cn, zhul@nanoctr.cn, yangyl@nanoctr.cn.

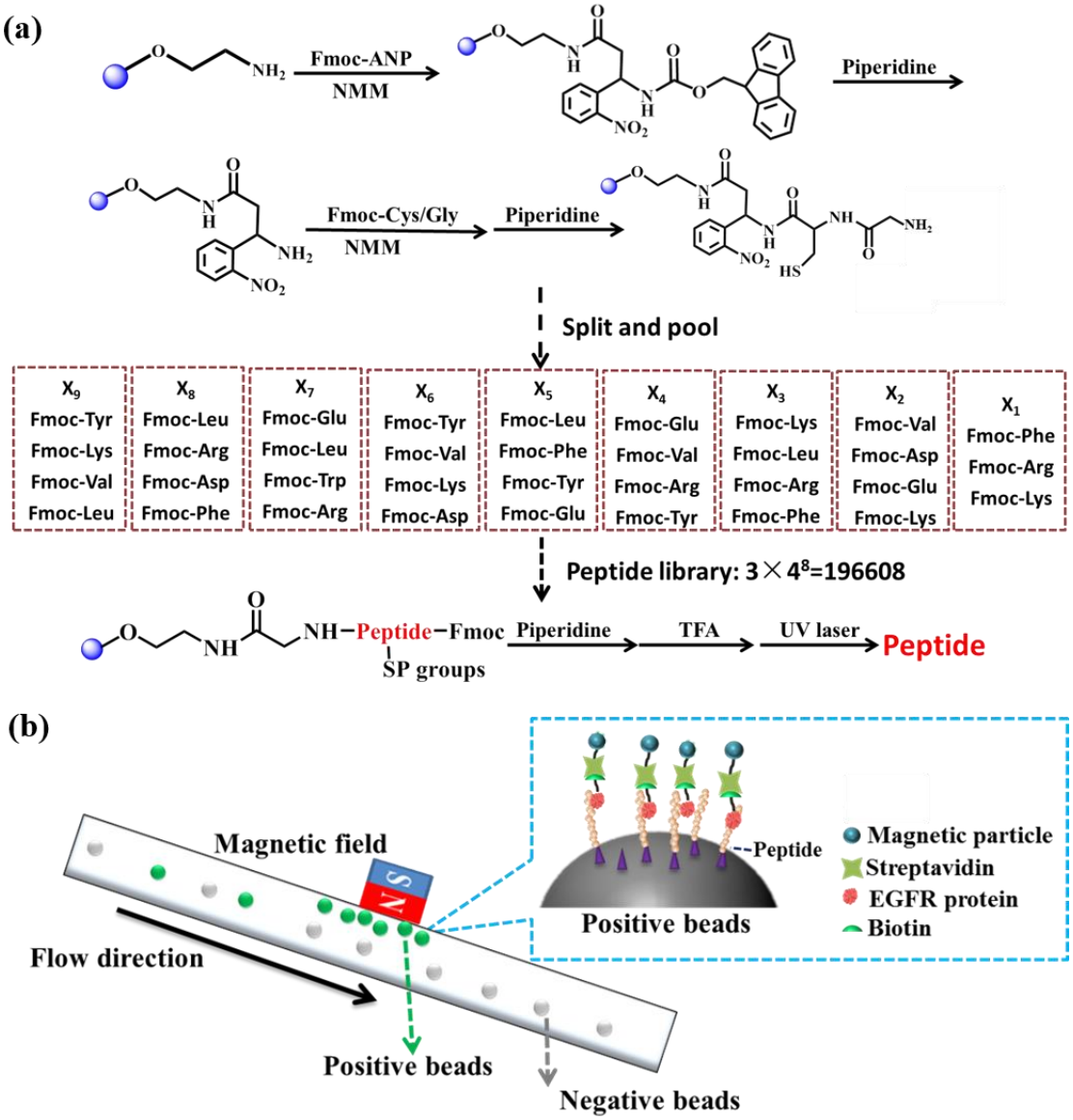

Scheme S1. Library construction and screening for EGFR-targeting peptides. (a) Construction and synthesis of the OBOC peptide library towards EGFR. (b) Schematic illustration of trapping and sorting of positive peptide beads through microchannel in the presence of magnetic field.

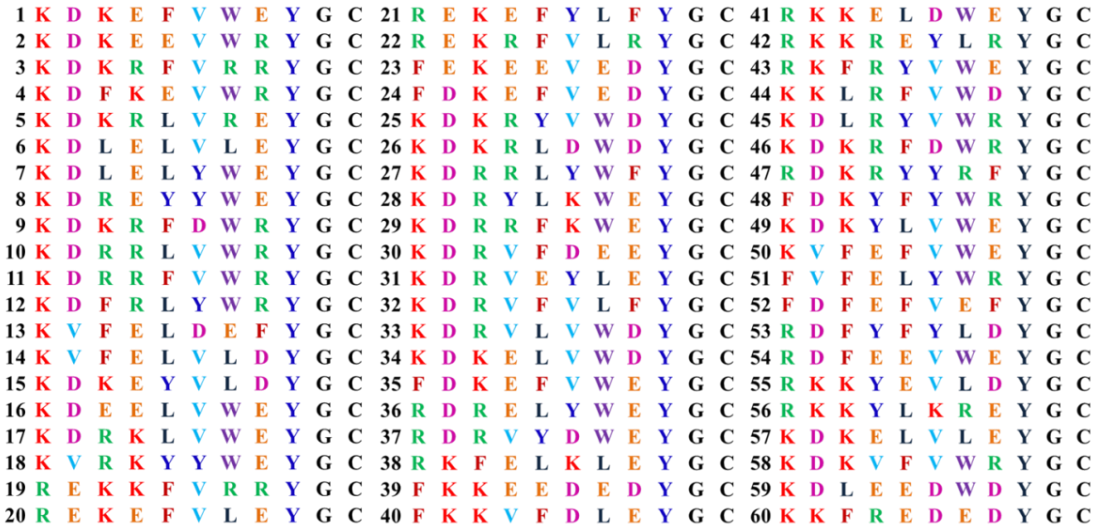

Figure S1. Sequence alignment of noncanonical EGFR binding peptides using the ClustalX2 multiple alignment tool.

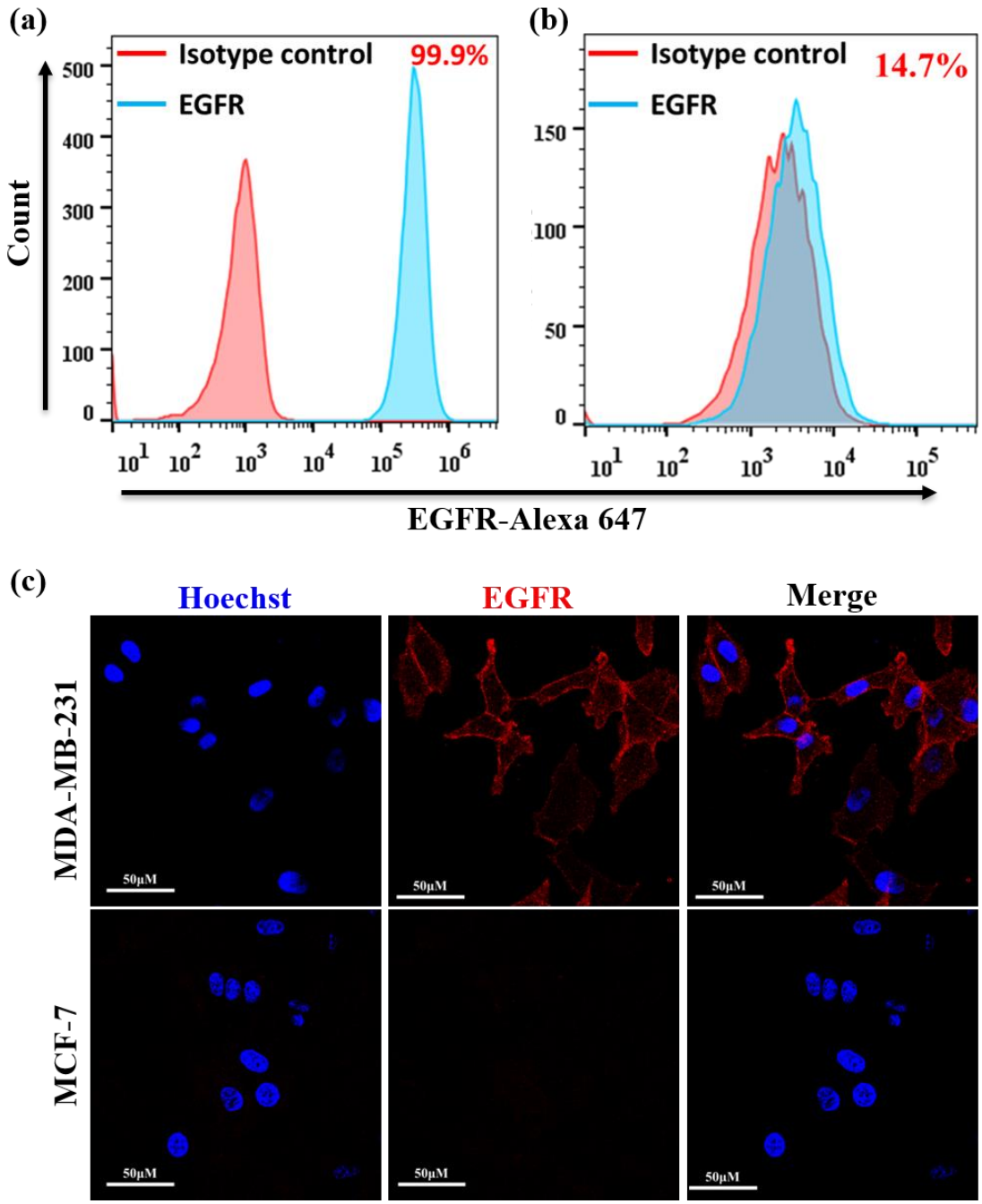

Figure S2. Evaluation of the expression of EGFR in MDA-MB-231 and MCF-7 cells. (a, b) Flow cytometry analysis of the expression of EGFR in (a) MDA-MB-231 and (b) MCF-7. Cells were labeled with anti-EGFR-Alexa 647. Isotype IgG was used as negative control. (c) Confocal microscopic images showing the expression of EGFR in MDA-MB-231 (upper) and MCF-7 (bottom). Cells were labeled with anti-EGFR-Alexa 647 and the nuclei stain DAPI. Scale bar: 50 μm.

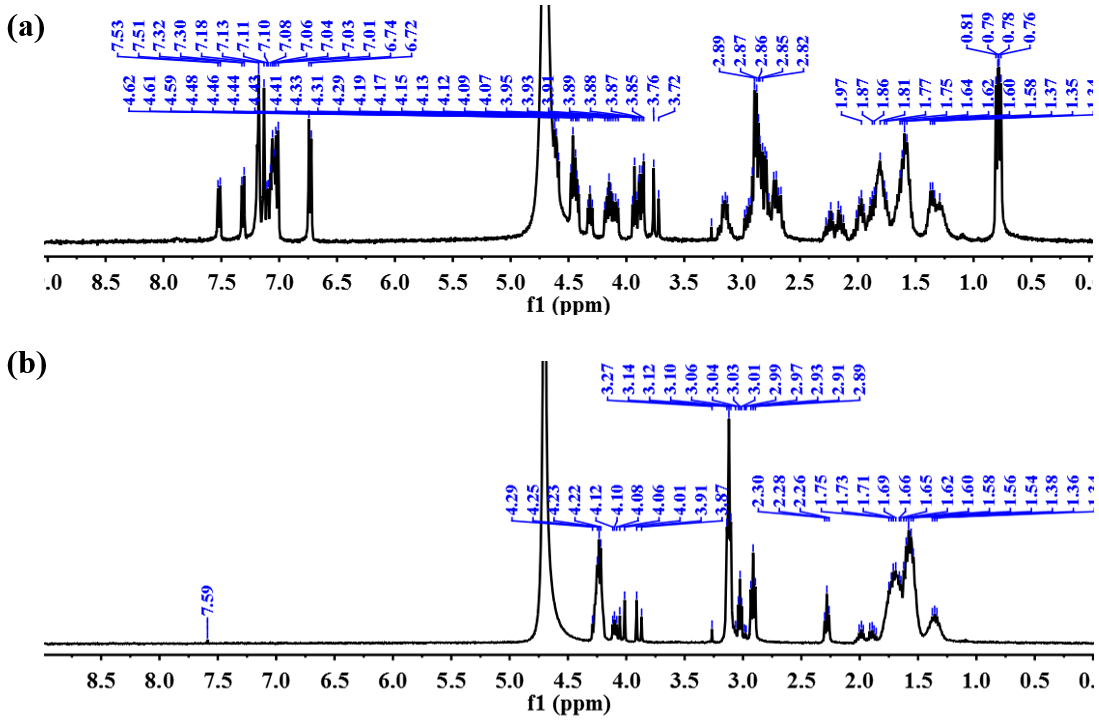

Figure S3. [1]HNMR spectrum of (a) EBP-1 peptide, (b) TAT-GC peptide in D_2O.

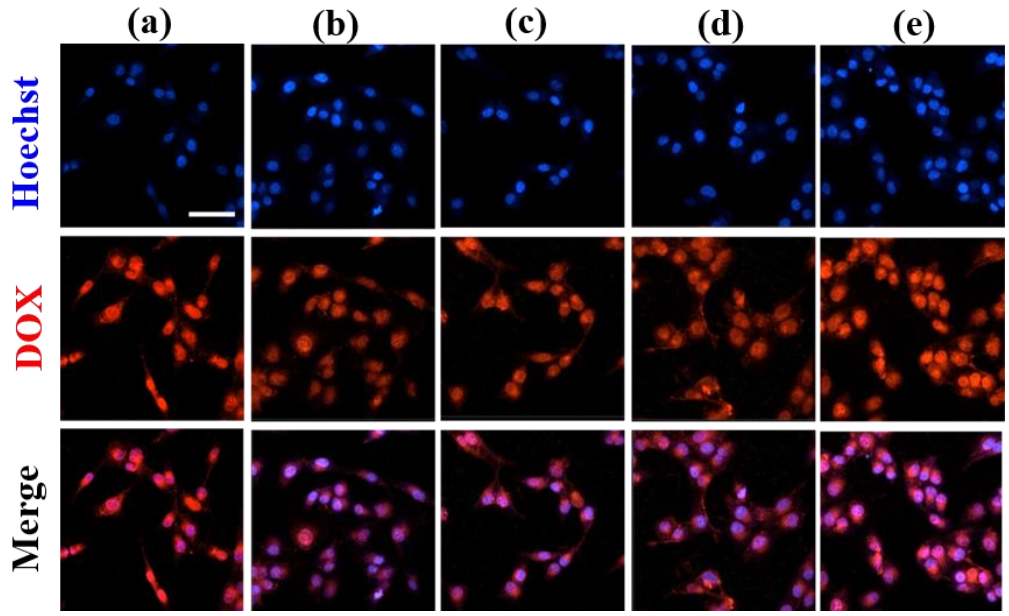

Figure S4. Cellular uptake of (a) free DOX, (b) PAMAM-PEG@DOX, (c) PAMAM-PEG-EBP1@DOX, (d) PAMAM-PEG-TAT@DOX and (e) PAMAM-PEG-EBP1-TAT@DOX in MDA-MB-231 cells detected by LCSM, scare bare: 50 μm.

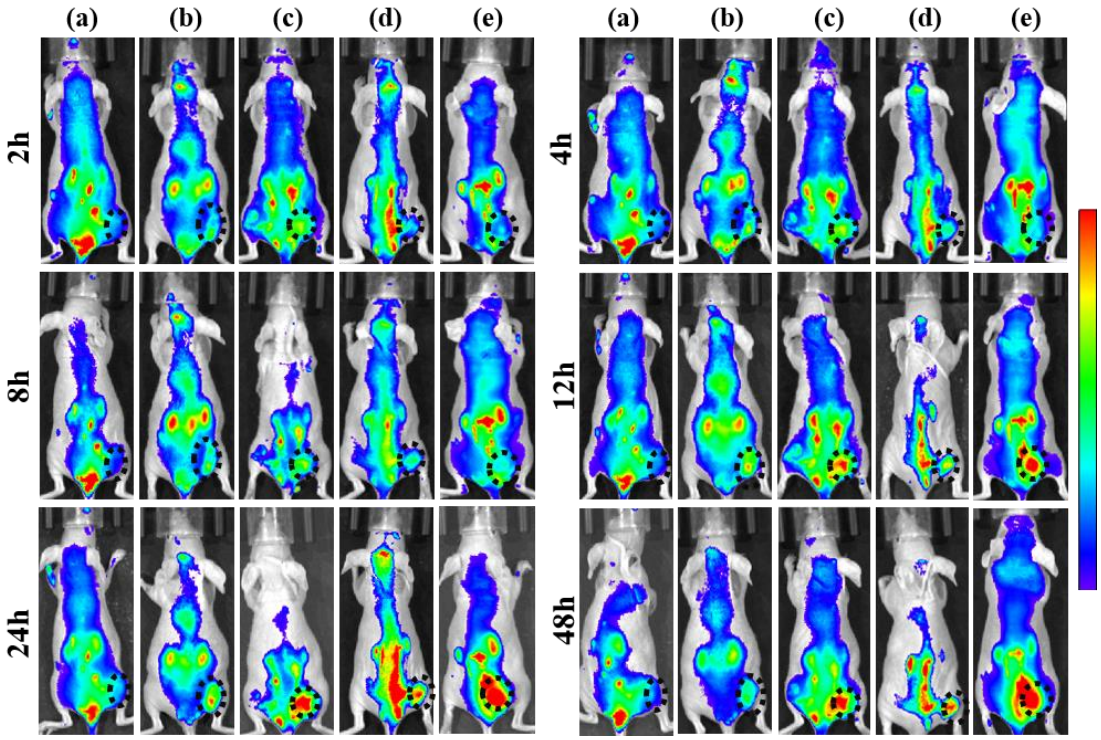

Figure S5. Targeting effect were detected by *in vivo* imaging system (IVIS Spectrum, USA) after accumulating for 2 h, 4 h, 8 h, 12 h, 24 h and 48 h. The breast cancer bearing mice were administrated with DiR-encapsulated dendrimers at a DiR dose of 2 mg/kg.

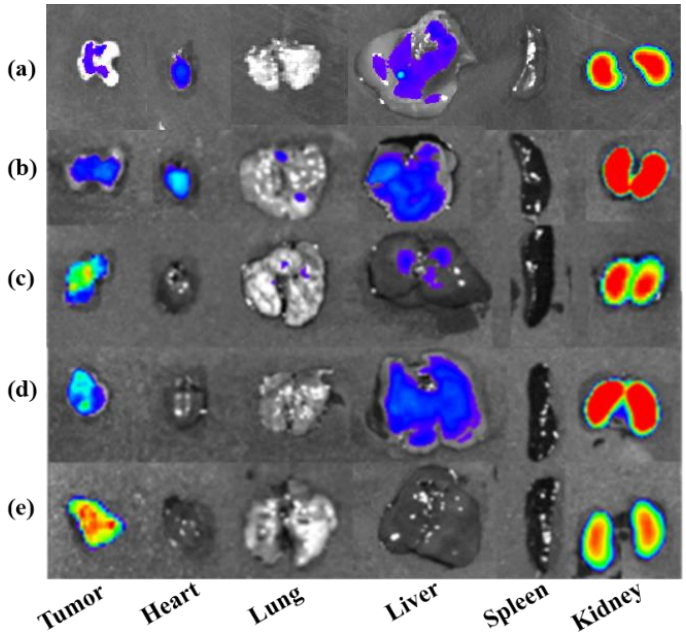

Figure S6. *Ex vivo* imaging of bio-distribution in major organs (heart, lung, liver, spleen and kidney) and tumor accumulation at 24 h after being administrated with (a) free DiR and DiR-loaded (b) PAMAM-PEG, (c) PAMAM-PEG-EBP1, (d) PAMAM-PEG-TAT, (e) PAMAM-PEG-EBP1-TAT at a DiR dose of 2 mg/kg.

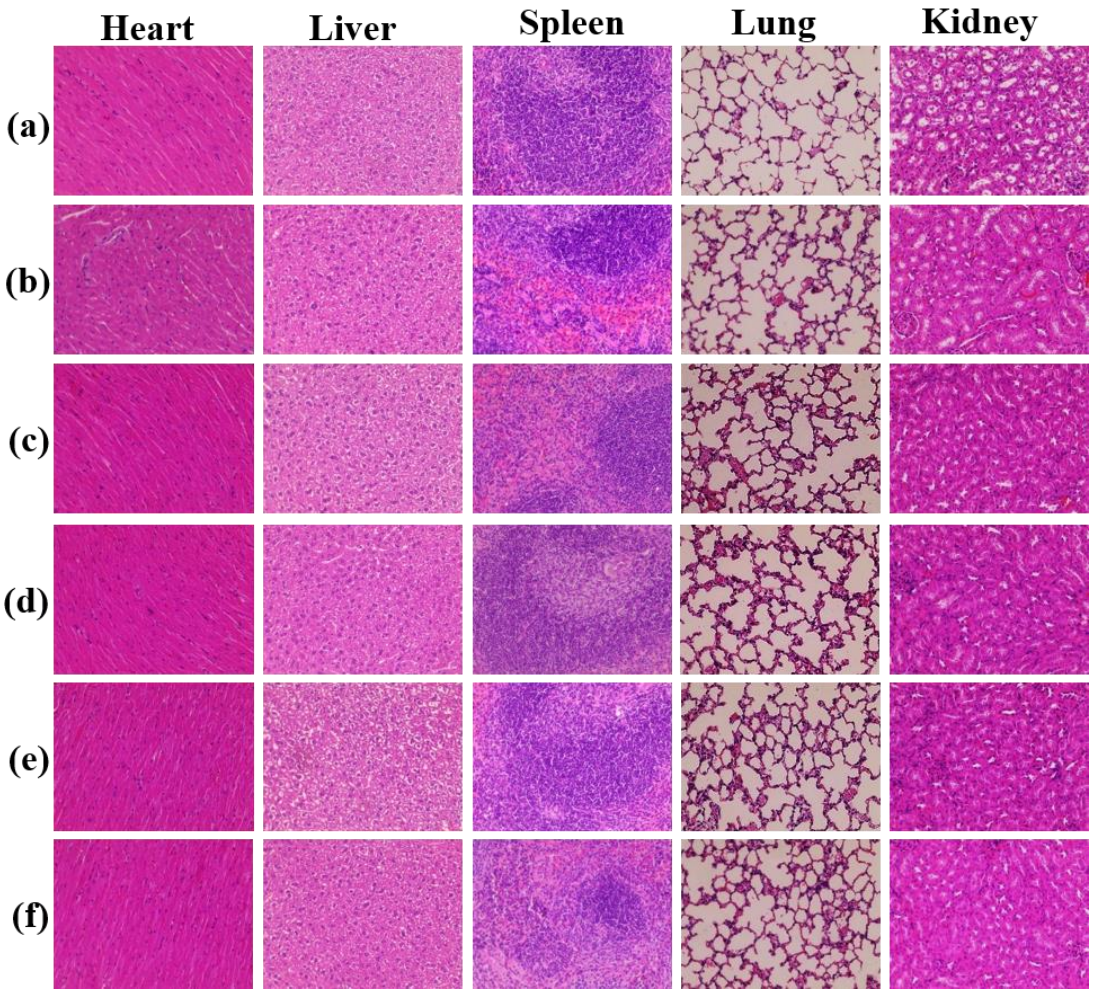

Figure S7. Histological analysis of tissues from major organs of female BALB/C mice after treatment with (a) saline, (b) free DOX, (c) PAMAM-PEG@DOX, (d) PAMAM-PEG-EBP1 @DOX, (e) PAMAM-PEG-TAT@DOX and (f) PAMAM-PEG-EBP1-TAT@DOX with 5mg kg^{-1} equivalent dose of DOX.

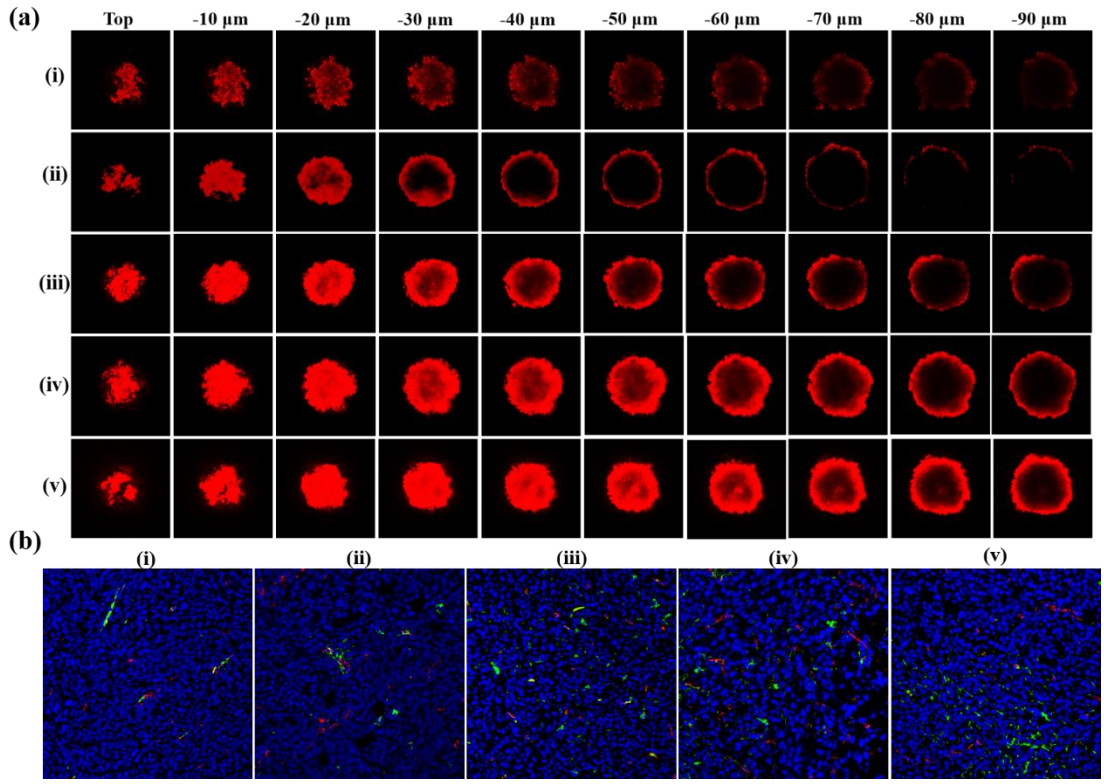

Figure S8. Penetration ability evaluation of (i) free DOX, (ii) PAMAM-PEG@DOX, (iii) PAMAM-PEG-EBP1@DOX, (iv) PAMAM-PEG-TAT@DOX and (v) PAMAM-PEG-EBP1-TAT@DOX. (a) Penetrability evaluation *in vitro* by LSCM Z-stack scanning. MDA-MB-231 multicellular spheroids were incubated with different DOX formulations at a DOX concentration of 20 μM for 5 h. (b) Immunofluorescence staining images of the intratumor distribution. Tumors were excised and cut into 10 μm slides after being administrated with free DOX and DOX loaded different carriers at a DOX dose of 5 mk/kg for 24 h. Tumor vessels were stained with Alexa 647-labeled CD31 antibody (red), nuclei were stained with DAPI (blue), and DOX were represented by green.